

1 **Extratropical intraseasonal signals along the subtropical westerly jet**
2 **as a window of opportunity for subseasonal prediction over East Asia**
3 **in boreal summer**

4
5 **Tao Zhu^{1,2} Jing Yang^{1,2}**
6
7

8 *¹ Key Laboratory of Environmental Change and Natural Disaster, Beijing Normal*
9 *University, Beijing 100875, China*

10 *² Faculty of Geographical Science, Beijing Normal University, Beijing 100875, China*
11

12
13
14
15
16 **Submitted to GRL**

17 **Nov. 2022**

18 **Corresponding author address: Jing Yang, Key Laboratory of Environmental Change*
19 *and Natural Disaster, Faculty of Geographical Science, Beijing Normal University,*

20 *19#Xinjiekouwai Street, Haidian District, Beijing 100875, China. E-mail:*

21 yangjing@bnu.edu.cn

22

Abstract

23 Previous studies suggest that boreal summer intraseasonal variations along the
24 subtropical westerly jet (SJ), featuring quasi-biweekly periodicity, frequently modulate
25 downstream subseasonal variations over East Asia (EA). Based on subseasonal
26 hindcasts from six dynamical models, this study discovered that the leading two–three-
27 week prediction skills for surface air temperature (SAT) are improved significantly in
28 summer when the SJ has strengthened intraseasonal signals, which are best
29 demonstrated over the eastern Tibetan Plateau, Southwest Basin, and North China. The
30 reasons are that the enhanced quasi-biweekly wave and the associated energy dispersion
31 along the SJ cause more regular quasi-biweekly periodic variations of downstream SAT,
32 which potentially increase regional predictability. This study suggests not only that
33 intraseasonal variations along the SJ could provide a window of opportunity for
34 achieving better subseasonal prediction over EA, but also that intraseasonal waves
35 along the SJ are crucial for improving EA subseasonal prediction.

36

Key Points

- 38 ● Subseasonal prediction skill over three key regions of China exhibits strong
39 dependence on the intensity of intraseasonal variations along the subtropical
40 westerly jet (SJ).
- 41 ● Enhanced intraseasonal waves and intensified energy dispersion along the SJ
42 increase regional surface air temperature predictability by strengthening local
43 periodic variations.
- 44 ● The intraseasonal signal along the SJ provides a window of opportunity for
45 subseasonal prediction of regional surface air temperature during boreal summer.

46

Plain Language Summary

47 Conventional opinion considers extratropical atmospheric perturbation as noise for
48 subseasonal-to-seasonal predictions. However, based on six state-of-the-art
49 subseasonal-to-seasonal hindcasts, this study established the groundbreaking result that
50 the subseasonal surface air temperature prediction skill, in three regions of China,
51 depends strongly on the intensity of extratropical intraseasonal variation along the
52 subtropical westerly jet. Breaking with the established perspective that the subseasonal
53 prediction source mainly comes from the tropical region, this study was the first to
54 propose that extratropical intraseasonal variation could provide a window of
55 opportunity for subseasonal prediction in regions of East Asia. The results suggest that
56 accurately capturing and predicting periodic extratropical atmospheric signals in
57 operational predictions will be of great importance for improving subseasonal
58 predictions of East Asian monsoon regions.

59 **1. Introduction**

60 Subseasonal prediction, which is crucial for many sectors of society and for
61 decision makers in terms of improved planning and preparations for saving lives,
62 protecting property, and increasing economic vitality (National Academies of Sciences
63 report 2016), is a challenging task in operational service (Robertson et al. 2015; Vitart
64 et al. 2017). One current barrier to improved subseasonal prediction is the obscure
65 prediction sources on this time scale. Previous studies have attempted to elucidate the
66 subseasonal prediction sources, including tropical intraseasonal oscillations (e.g., the
67 Madden–Julian Oscillation (MJO) and boreal summer intraseasonal oscillation
68 (BSISO)), anomalous signals from land (soil moisture and soil temperature), snow
69 cover, sea ice, the stratosphere, and the ocean (e.g., the El Niño–Southern Oscillation
70 (ENSO), local sea surface temperature, and mesoscale sea surface temperature
71 variability), which have all been reviewed comprehensively in the National Academies
72 of Sciences report (2016) and Merryfield et al. (2020).

73 Skillful subseasonal prediction is particularly important over East Asia (EA),
74 which is one of the most densely populated regions globally, accounting for 22% of the
75 world’s population (Leung 2012). Subseasonal prediction in boreal summer over EA is
76 challenging owing to complex interactions between tropical monsoon variability and
77 mid–high-latitude circulation systems (Liang and Lin 2017). Previous studies proved
78 that subseasonal prediction sources over EA include preferable phases of the MJO (Lin
79 2018) and BSISO (Wu et al. 2022), the ENSO state (Martin et al. 2019), snowpack
80 (Orsolini et al. 2013; Li et al. 2020), land surface conditions (Zeng and Yuan 2018; Xie
81 et al. 2019; Xue et al. 2021) and stratospheric signals (Yu et al. 2021). Conventional
82 perspective considers the extratropical atmospheric perturbation as noise for prediction
83 (Vimont et al. 2001; Zhang et al. 2018). However, along the subtropical westerly jet
84 (SJ), remarkable periodic atmospheric intraseasonal signals, such as a quasi-biweekly
85 oscillation, have been proven to have significant influence on the weather and climate
86 of EA (Watanabe and Yamazaki 2012; Yang et al. 2017; Zhong et al. 2022) and even
87 to trigger extreme events (Chan et al. 2002; Fujinamij and Yasunari 2004; Li et al. 2021).

88 Meanwhile, a number of recent studies have found that subseasonal prediction biases
89 over EA are affected substantially by extratropical intraseasonal oscillations along the
90 SJ (EISO-SJ) (Qi and Yang 2019; Yan et al. 2021, 2022). Therefore, it is worth
91 investigating whether the atmospheric EISO-SJ, similar to the MJO/BSISO, is one of
92 the subseasonal prediction sources over EA.

93 Considering the atmospheric EISO-SJ features remarkable year-to-year variation
94 in boreal summer (Fig. S1 in the supplementary materials presents a simple example
95 examining the year-to-year variation of the intraseasonal SJ index, calculated in
96 accordance with the definition of Yang and Zhang (2007)), the objective of this study
97 was to investigate whether there exists remarkable dependence of EA subseasonal
98 prediction on the atmospheric EISO-SJ from the perspective of comparing summers
99 with strong and weak EISO-SJ intensity, primarily based on the subseasonal-to-
100 seasonal (S2S) hindcast dataset. The results presented in this paper are analyzed in an
101 attempt to identify another important window of opportunity for EA subseasonal
102 prediction.

103 **2. Data and methods**

104 Daily atmospheric circulation fields were retrieved from the ERA-Interim dataset
105 provided by the European Centre for Medium-Range Weather Forecasts (ECMWF)
106 (Dee et al., 2011). The horizontal resolution of the gridded data was $1.5^{\circ} \times 1.5^{\circ}$ and the
107 historical record covered 1982–2018. Daily surface air temperature (SAT) and
108 precipitation data (1982–2018) recorded at 2479 observing stations in China were
109 obtained from the China Meteorological Administration. Here, boreal summer is
110 defined as May 1 to August 31.

111 For the S2S reforecast data, the hindcast from the database of the S2S prediction
112 project was used (Virart et al. 2017), in which six models were analyzed: the China
113 Meteorological Administration (CMA), the European Center for Medium-Range
114 Forecast (ECMWF), the Environment and Climate Change Canada (ECCC), the
115 Institute of Atmospheric Sciences and Climate of the National Research Council
116 (ISAC-CNR), the Meteo-France/Centre National de Recherche Meteorologiques

117 (Meteo-France), and the National Centers for Environmental Prediction (NCEP). A
118 detailed description of each of the six models is presented in Table S1 in the
119 supplementary materials. Note that the purpose of this study was not to compare model
120 prediction skill, but to understand the dependence of EA subseasonal prediction on the
121 atmospheric EISO-SJ. Therefore, there was no requirement for the reforecast period,
122 frequency of initialization, and ensemble size of the models to be uniform. Also note
123 that the prediction skills for weekly SAT and precipitation were our targets, for which
124 the weekly hindcast data could be obtained from the 7-day mean of the raw prediction
125 data. For example, a two-week (three-week) prediction corresponds to the average of
126 the forecast 11–17 (18–24) days.

127 The intraseasonal component of a particular variable can be obtained by the
128 following two steps: I) subtracting the climatological mean and the first three harmonics,
129 and II) taking a 5-day running mean. The quasi-biweekly (8–25 days in this study)
130 component can be retrieved easily using the Butterworth bandpass filter. The statistical
131 methods used in this study included empirical orthogonal function analysis and power
132 spectrum analysis. A two-tailed Student's t test was used to assess statistical
133 significance. Evaluation methods included the temporal correlation skill (TCC), root
134 mean square error (RMSE), and relative operating characteristics (ROC) curve, which
135 are the primary and most commonly used methods for evaluating the prediction skill of
136 S2S models (Black et al. 2017; Wu et al. 2017; Osman and Alvarez 2018). A larger
137 (smaller) TCC (RMSE) value represents better deterministic prediction skill, and a
138 larger value of the area under the ROC curve (named ROCA), denotes better
139 probabilistic prediction skill. Full details of the calculation methods can be found in
140 Table S2 and Eqs. (S1) and (S2) in the supplementary materials. Two-dimensional
141 wave activity flux, which is used to represent the energy dispersion of a Rossby wave,
142 was calculated with reference to Takaya and Nakamura (2001).

143 **3. Remarkable year-to-year variation in EISO-SJ intensity**

144 Similar to some previous studies on the year-to-year variation of intraseasonal
145 oscillation (e.g., Teng and Wang 2003; Moon et al. 2011; Qin et al. 2022), EISO-SJ

146 intensity is measured by the standard deviation of boreal summer quasi-biweekly 200
147 hPa meridional wind (V200) averaged over the SJ core region (35° – 43° N, 83° – 98° E;
148 shown by the black rectangle in Fig. 1b), i.e., the maximum center of both quasi-
149 biweekly V200 variance and fractional variance (nearly 45% of the total variance) (Figs.
150 1a and 1b). In this study, V200 was chosen as the typical variable for representing the
151 EISO-SJ because it features more prominent intraseasonal signals than other circulation
152 fields (e.g., 200 hPa geopotential height (GHT200) and zonal wind (U200)) along the
153 SJ (Figs. S2a–f in the supplementary materials). The quasi-biweekly component was
154 extracted to represent intraseasonal V200 because it is the most dominant intraseasonal
155 periodicity according to the power spectra of the circulation fields along the SJ (Fig.
156 S2g in the supplementary materials).

157 Figure 1c displays the year-to-year variation of EISO-SJ intensity. First, EISO-SJ
158 intensity exhibits significant year-to-year variation, in which the difference between the
159 maximum and minimum value is 3.18, which represents 72.5% of the total V200
160 intensity (4.39). Second, EISO-SJ intensity has a significant relationship with the year-
161 to-year change in total V200 intensity along the SJ, for which the correlation coefficient
162 is up to 0.51, far exceeding the 99% significance level. Meanwhile, the year-to-year
163 fractional variance of EISO-SJ intensity (variance: $0.56 \text{ m}^2 \text{ s}^{-2}$) against the total V200
164 intensity (variance: $0.87 \text{ m}^2 \text{ s}^{-2}$) is 64.0%. The above results show that EISO-SJ
165 intensity has large year-to-year variation that is highly consistent with the year-to-year
166 variation of total V200 intensity.

167 To probe the dependence of EA subseasonal prediction on the atmospheric EISO-
168 SJ, two contrasting groups of summers were evaluated for each specific S2S model:
169 strong EISO-SJ summers (EISO-SJ-S) and weak EISO-SJ summers (EISO-SJ-W).
170 Taking the ECMWF as an example, because the reforecast period is 1996–2015 and the
171 frequency of initialization is twice a week, the five strongest EISO-SJ intensity
172 summers (2004, 2007, 2009, 2011, and 2013) in terms of the observations were chosen
173 for the EISO-SJ-S group, and the five weakest EISO-SJ intensity summers (1998, 2003,
174 2008, 2010, and 2012) in terms of the observations were taken as the EISO-SJ-W group.

175 The sample size of each group was 175 (5 years \times 35 times year⁻¹). Analysis for the
176 other models followed similar methods and detailed descriptions can be found in Table
177 S1 in the supplementary materials. To ensure distinct differences between the two
178 groups and to maintain adequate sample sizes, the selected EISO-SJ-S and EISO-SJ-W
179 summers exceeded a threshold of at least 0.7 times the standard deviation.

180 **4. Dependence of subseasonal prediction for EA SAT on the EISO-SJ**

181 Previous observational studies reported that atmospheric EISO-SJ is crucial for
182 subseasonal variation in EA SAT (Watanabe and Yamazaki 2014; Gao et al. 2017).
183 Therefore, in this section, we first focus on exploring the differences in the subseasonal
184 prediction skill for EA SAT between the EISO-SJ-S and EISO-SJ-W summers.
185 Comparison is made for both deterministic (TCC and RMSE) and probabilistic
186 prediction (ROC) to verify the results. Two- and three-week lead predictions are the
187 focuses of this study because the skill beyond four weeks is poor for both groups of
188 summers. Three typical regions are chosen (eastern Tibetan Plateau (ETP): 29°–37°N,
189 89°–104°E, Southwest Basin (SWB): 24°–29°N, 101°–109°E, and North China (NC):
190 38°–44°N, 109°–119°E; black frames in Fig. S3 in the supplementary materials)
191 because the raw SAT anomaly over these regions exhibits significant correlation with
192 the domain-averaged quasi-biweekly V200 over the SJ core.

193 4.1 Better subseasonal deterministic prediction for EA SAT in summers with strong 194 EISO-SJ intensity

195 The TCC and RMSE were calculated to measure the similarity and magnitude of
196 the error between the predicted and observed weekly SAT anomaly (Harnos et al. 2019).
197 Figures 2a–c shows the TCCs between the observed weekly SAT anomaly and the
198 predicted ensemble-mean anomalies with two- and three-week lead times from the six
199 S2S models over the ETP, SWB, and NC in EISO-SJ-S and EISO-SJ-W summers. The
200 TCCs for all six S2S models are larger for EISO-SJ-S summers than for EISO-SJ-W
201 summers in all three regions. For a three-week lead prediction over the ETP, the TCCs
202 are 0.34 (ECMWF), 0.15 (CMA), 0.44 (Meteo-France), 0.34 (NCEP), 0.17 (ECCC),
203 and 0.23 (ISAC-CNR) for EISO-SJ-S summers, while 0.23 (ECMWF), 0.08 (CMA),

204 0.13 (Meteo-France), 0.11 (NCEP), 0.10 (ECCC), and 0.05 (ISAC-CNR) for EISO-SJ-
205 W summers (green bars in Fig. 2a). Similarly, the TCCs for EISO-SJ-S summers
206 decrease from 0.50 to 0.01 (ECMWF), 0.17 to 0.01 (CMA), 0.34 to 0.12 (Meteo-
207 France), 0.20 to 0.17 (NCEP), 0.29 to 0.04 (ECCC), and 0.19 to -0.02 (ISAC-CNR) for
208 EISO-SJ-W summers over the SWB (green bars in Fig. 2b), and the TCCs are reduced
209 from 0.36 (ECMWF), 0.12 (CMA), 0.32 (Meteo-France), 0.27 (NCEP), 0.17 (ECCC)
210 and 0.14 (ISAC-CNR) for EISO-SJ-S summers to 0.29 (ECMWF), 0.09 (CMA), 0.21
211 (Meteo-France), 0.12 (NCEP), 0.04 (ECCC), and 0.06 (ISAC-CNR) for EISO-SJ-W
212 summers over NC (green bars in Fig. 2c). Similar differences can be seen clearly in the
213 two-week lead predictions, although the differences between EISO-SJ-S and EISO-SJ-
214 W summers are not as significant as those in three-week lead predictions (see red bars
215 in Figs. 2a–c).

216 The RMSEs of the six S2S models for the predicted weekly SAT anomaly against
217 the observations over each of the three domains are shown in Figs. 2d–f. The RMSEs
218 for all six S2S models are smaller for EISO-SJ-S summers than for EISO-SJ-W
219 summers. Quantitatively, for a three-week lead prediction over the ETP, the RMSEs
220 are 0.92 (ECMWF), 1.16 (CMA), 0.92 (Meteo-France), 1.03 (NCEP), 1.13 (ECCC),
221 and 1.15 (ISAC-CNR) for EISO-SJ-S summers. In contrast, for EISO-SJ-W summers,
222 the RMSEs are 0.96 (ECMWF), 1.18 (CMA), 1.03 (Meteo-France), 1.12 (NCEP), 1.14
223 (ECCC), and 1.16 (ISAC-CNR) (blue bars in Fig. 2d). Over the SWB, the increase in
224 RMSEs from EISO-SJ-S summers to EISO-SJ-W summers is from 1.03 to 1.13
225 (ECMWF), 1.34 to 1.35 (CMA), 1.08 to 1.14 (Meteo-France), 1.13 to 1.27 (NCEP),
226 1.33 to 1.36 (ECCC), and 1.15 to 1.41 (ISAC-CNR) (blue bars in Fig. 2e). Over NC,
227 the RMSEs are increased from 1.23 (ECMWF), 1.49 (CMA), 1.21 (Meteo-France),
228 1.30 (NCEP), 1.62 (ECCC), and 1.52 (ISAC-CNR) for EISO-SJ-S summers to 1.36
229 (ECMWF), 1.61 (CMA), 1.30 (Meteo-France), 1.42 (NCEP), 1.71 (ECCC), and 1.61
230 (ISAC-CNR) for EISO-SJ-W summers (green bars in Fig. 2f). Similarly, two-week lead
231 predictions show similar contrasting features (yellow bars in Figs. 2d–f). The unified
232 differences over the three regions for all six S2S models, based on both TCCs and

233 RMSEs, demonstrate that the deterministic prediction skills for the weekly SAT
234 anomaly over EA are significantly better in summers with strong EISO-SJ intensity
235 than in summers with weak EISO-SJ intensity.

236 4.2 Better subseasonal probabilistic prediction for EA SAT in summers with strong 237 EISO-SJ intensity

238 The ROC curve is used to comprehensively evaluate model performance in
239 simulating the probability of occurrence of above-normal SAT events. Here, an above-
240 normal SAT event is defined as a weekly SAT warm anomaly of >1 °C (Wu et al. 2017).
241 The ROC curves for the six S2S models for predicted above-normal SAT events over
242 the ETP, SWB, and NC are shown in Fig. 3, respectively, in EISO-SJ-S and EISO-SJ-
243 W summers. Obviously, the six S2S models have larger ROCAs for EISO-SJ-S
244 summers than for EISO-SJ-W summers over each of the three regions. In terms of the
245 three-week lead prediction over the ETP, the ROCAs are 0.62 (ECMWF), 0.57 (CMA),
246 0.65 (Meteo-France), 0.65 (NCEP), 0.61 (ECCC), and 0.61 (ISAC-CNR) for EISO-SJ-
247 S summers, while 0.61 (ECMWF), 0.54 (CMA), 0.57 (Meteo-France), 0.60 (NCEP),
248 0.55 (ECCC), and 0.58 (ISAC-CNR) for EISO-SJ-W summers (green solid and dotted
249 lines in Fig. 3a). Over the SWB, the ROCAs decrease from 0.64 (ECMWF), 0.57
250 (CMA), 0.59 (Meteo-France), 0.60 (NCEP), 0.66 (ECCC), and 0.56 (ISAC-CNR) for
251 EISO-SJ-S summers to 0.52 (ECMWF), 0.52 (CMA), 0.52 (Meteo-France), 0.58
252 (NCEP), 0.45 (ECCC), and 0.55 (ISAC-CNR) for EISO-SJ-W summers (green solid
253 and dotted lines in Fig. 3b). Over NC, the ROCAs decrease from 0.74 (ECMWF), 0.54
254 (CMA), 0.67 (Meteo-France), 0.65 (NCEP), 0.54 (ECCC), and 0.58 (ISAC-CNR) for
255 EISO-SJ-S summers to 0.53 (ECMWF), 0.53 (CMA), 0.60 (Meteo-France), 0.55
256 (NCEP), 0.50 (ECCC), and 0.49 (ISAC-CNR) for EISO-SJ-W summers (green solid
257 and dotted lines in Fig. 3c). The two-week lead ROCAs show similar differences
258 between EISO-SJ-S and EISO-SJ-W summers (red solid and dotted lines in Fig. 3). We
259 also performed similar analysis for below-normal and normal SAT events, and the
260 results revealed similar differences (Fig. S4 in the supplementary materials). The results
261 from the evaluation of probabilistic prediction also clearly exhibited that the prediction

262 skills with two- and three-week lead times are evidently improved when EISO-SJ
263 intensity is enhanced in summer.

264 4.3 Dependence of subseasonal prediction for EA SAT on the EISO-SJ is independent 265 of ENSO/MJO/BSISO

266 Considering that subseasonal prediction for EA SAT is likely modulated by the
267 mean state such as ENSO (Martin et al. 2019) and tropical intraseasonal oscillation such
268 as the MJO (e.g., Liang and Lin 2017; Lin 2018) and BSISO (Wu et al. 2022), we
269 reexamined the robustness of the above results by removing ENSO/MJO/BSISO-
270 associated summers (Table S3 in the supplementary materials lists the new samples of
271 each model after the elimination of ENSO/MJO/BSISO-associated summers).
272 Excluding the impact from ENSO, MJO, and BSISO, the subseasonal prediction for
273 SAT also exhibits better skill in EISO-SJ-S summers than in EISO-SJ-W summers
274 (Figs. S5–6 in the supplementary materials). The results indicate that the strong
275 dependence of subseasonal prediction for EA SAT on the EISO-SJ, identified as a new
276 finding in this study, is independent of ENSO/MJO/BSISO.

277 Therefore, the high level of agreement among the six S2S models and three target
278 regions, with respect to better prediction skill in summers with strong EISO-SJ intensity
279 in comparison with that in summers with weak EISO-SJ intensity, strongly suggests
280 that the amplified quasi-biweekly periodic signals along the SJ evidently increase the
281 regional subseasonal predictability over EA.

282 5. Discussion

283 Previous studies reported that the EISO-SJ mainly features a zonal quasi-biweekly
284 Rossby wave in boreal summer (Fujinami and Yasunari 2004; Yang et al. 2014, 2017).
285 We therefore considered the empirical orthogonal function for the quasi-biweekly V200
286 over the SJ region in EISO-SJ-S and EISO-SJ-W summers, and regressed the
287 corresponding quasi-biweekly V200 and 200 hPa wave activity flux on the first
288 principal component, as shown in Figs. 4a and 4b, respectively. There are clear Rossby
289 waves in both EISO-SJ-S and EISO-SJ-W summers along the SJ, but the stronger wave
290 activity fluxes propagate eastward along the SJ toward EA, significantly enhancing the

291 quasi-biweekly signals in that regions in EISO-SJ-S summers in comparison with those
292 in EISO-SJ-W summers. Furthermore, the variances of quasi-biweekly SAT are larger
293 over the ETP, SWB, and NC in EISO-SJ-S summers than in EISO-SJ-W summers (Fig.
294 4c). The results suggest that the quasi-biweekly Rossby wave and the associated energy
295 dispersion along the SJ are enhanced (reduced) over EA in EISO-SJ-S (EISO-SJ-W)
296 summers, causing stronger (weaker) quasi-biweekly periodic variations in the target
297 regional SAT. This can explain why the two- and three-week lead predictions in the
298 S2S hindcast are improved remarkably in EISO-SJ-S summers.

299 We also performed similar analysis for precipitation, but failed to find significant
300 dependence on EISO-SJ (not shown). We investigated the reason why subseasonal
301 prediction of EA precipitation might be insensitive to EISO-SJ intensity. Table S4 in
302 the supplementary materials lists the fractional variances of quasi-biweekly and
303 synoptic (i.e., below-8-day) components for SAT and precipitation over the ETP, SWB,
304 and NC. Interestingly, for SAT, the fractional variance of the quasi-biweekly
305 component is much larger than that of the synoptic component (e.g., the three region-
306 averaged quasi-biweekly fractional variance is 39.1%, which is twice that of the
307 synoptic component). For precipitation, however, the fractional variance of the quasi-
308 biweekly component is smaller than that of the synoptic component (31.9% versus 39.2%
309 on average). The above results indicate that the footprint of the atmospheric EISO-SJ
310 on the subseasonal variation of precipitation is not as significant as that on the SAT
311 over EA, which also suggests that subseasonal prediction for EA precipitation is more
312 difficult than that for EA SAT.

313 **6. Conclusions**

314 Using hindcast data from six S2S models, this study found that the subseasonal
315 prediction skill for EA SAT exhibits evident dependence on the intensity of
316 intraseasonal variations along the SJ. In summers with strong EISO-SJ intensity, the
317 two–three-week prediction skills for SAT over the ETP, SWB and NC are significantly
318 better than those in summers with weak EISO-SJ intensity. Moreover, the strong
319 dependence of subseasonal prediction for EA SAT on EISO-SJ intensity is proven

320 independent of ENSO/MJO/BSISO. Further analysis indicated that the SJ-related
321 quasi-biweekly Rossby wave and the associated energy dispersion are significantly
322 strengthened downstream in strong EISO-SJ summers, resulting in stronger quasi-
323 biweekly signals propagating toward EA. These enhanced periodic signals would cause
324 more regular quasi-biweekly periodic variations in EA SAT, and increase regional
325 subseasonal predictability. However, subseasonal prediction for EA precipitation is
326 more difficult than that for EA SAT primarily because of the stronger internal synoptic
327 variability. This study demonstrated that intraseasonal variations along the SJ provide
328 a window of opportunity for subseasonal prediction of SAT over some regions of EA.
329 Meanwhile, this study suggests that accurately capturing and predicting extratropical
330 periodic atmospheric waves along the SJ in dynamic predictions will be of great
331 importance for improving subseasonal prediction over EA.

332 **Acknowledgments**

333 JY and TZ were supported by funds from the National Natural Science Foundation of
334 China (Grant No. 42022034) and the Key Collaborative Research Program of Alliance
335 of International Science Organizations (Grant No. ANSO-CR-2020-01). The authors
336 are grateful for the high-performance computing support from the Center for Geodata
337 and Analysis, Faculty of Geographical Science, Beijing Normal University.

338 **Data Availability Statement**

339 The ERA-Interim reanalysis data can be freely accessed via
340 <http://apps.ecmwf.int/datasets/data/interim-full-daily/levtype=sfc/>. The S2S hindcast
341 data are available from <https://apps.ecmwf.int/datasets/data/s2s/levtype=sfc/type=cf/>.
342 And the SAT and precipitation data recorded at 2479 observing stations are from
343 <http://data.cma.cn/en/?r=site/index> (only available by the registered members), and are
344 also obtained from the backup address (IP: 172.16.212.233:~/mnt/2479_station).

345 **References**

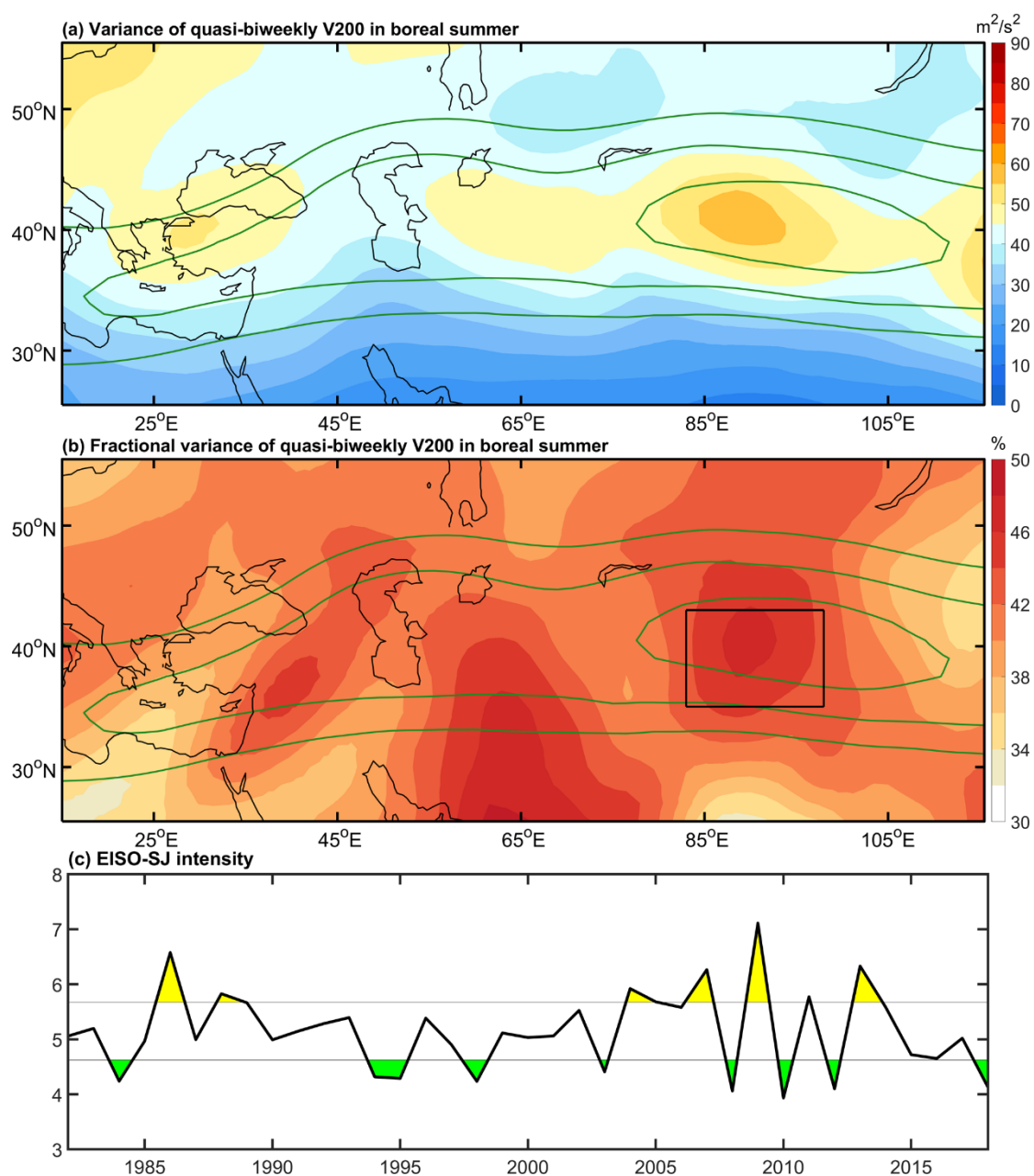
- 346 Black, J., Johnson, N. C., Baxter, S., Feldstein, S. B., Harnos, D. S., and L'Heureux, M.
347 L. (2017). The Predictors and Forecast Skill of Northern Hemisphere
348 Teleconnection Patterns for Lead Times of 3-4 Weeks. *Monthly Weather Review*,
349 *145*(7), 2855-2877. <https://doi.org/10.1175/MWR-D-16-0394.1>
- 350 Chan, J. C. L., Wi, W. X., and Xu, J. J. (2002). Mechanisms responsible for the
351 maintenance of the 1998 South China Sea Summer Monsoon. *Journal of the*
352 *Meteorological Society of Japan*, *80*(5), 1103-1113.
353 <https://doi.org/10.2151/jmsj.80.1103>
- 354 Dai, G. K., Mu, M., Li, C. X., Han, Z., and Wang, L. (2021). Evaluation of the Forecast
355 Performance for Extreme Cold Events in East Asia With Subseasonal-to-Seasonal
356 Data Sets From ECMWF. *Journal of Geophysical Research: Atmospheres*, *126*(1).
357 <https://doi.org/10.1029/2020JD033860>
- 358 Dee, D. P., et al. (2011). The ERA-Interim reanalysis: configuration and performance
359 of the data assimilation system. *Quarterly Journal of the Royal Meteorological*
360 *Society*, *137*(656), 553-597. <https://doi.org/10.1002/qj.828>
- 361 Fujinami, H., and Yasunari, T. (2004). Submonthly variability of convection and
362 circulation over and around the Tibetan Plateau during the boreal summer. *Journal*
363 *of the Meteorological Society of Japan*, *82*(6), 1545-1564.
364 <https://doi.org/10.2151/jmsj.82.1545>
- 365 Gao, M. N., Yang, J., Wang, B., Zhou, S. Y., Gong, D. Y., and Kim, S. J. (2018). How
366 are heat waves over Yangtze River valley associated with atmospheric quasi-
367 biweekly oscillation? *Climate Dynamics*, *51*(11-12), 4421-4437.
368 <https://doi.org/10.1007/s00382-017-3526-z>
- 369 Harnos, K. J., L'Heureux, M., Ding, Q., and Zhang, Q. (2019). Skill of Seasonal Arctic
370 Sea Ice Extent Predictions Using the North American Multimodel Ensemble.
371 *Journal of Climate*, *32*(2), 623-638. <https://doi.org/10.1175/JCLI-D-17-0766.1>

- 372 Leung, Y. F. (2012). Recreation ecology research in East Asia's protected areas:
373 Redefining impacts? *Journal for Nature Conservation*, 20(6), 349-356.
374 <https://doi.org/10.1016/j.jnc.2012.07.005>
- 375 Li, J. Y., Li, F., and Wang, H. J. (2020). Subseasonal prediction of winter precipitation
376 in southern China using the early November snowpack over the Urals.
377 *Atmospheric and Oceanic Science Letters*, 13(6), 534-541.
378 <https://doi.org/10.1080/16742834.2020.1824547>
- 379 Li, J. Y., Zhai, P. M., Mao, J. Y., Song, L. L., and Xiao, Q. Y. (2021). Synergistic Effect
380 of the 25-60-day Tropical and Midlatitude Intraseasonal Oscillations on the
381 Persistently Severe Yangtze Floods. *Geophysical Research Letters*, 48(20).
382 <https://doi.org/10.1029/2021GL095129>
- 383 Liang, P., and Lin, H. (2018). Sub-seasonal prediction over East Asia during boreal
384 summer using the ECCO monthly forecasting system. *Climate Dynamics*, 50(3-4),
385 1007-1022. <https://doi.org/10.1007/s00382-017-3658-1>
- 386 Lin, H. (2018). Predicting the Dominant Patterns of Subseasonal Variability of
387 Wintertime Surface Air Temperature in Extratropical Northern Hemisphere.
388 *Geophysical Research Letters*, 45(9), 4381-4389.
389 <https://doi.org/10.1029/2018GL077509>
- 390 Martin, G. M., Chevuturi, A., Comer, R. E., Dunstone, N. J., Scaife, A. A., and Zhang,
391 D. Q. (2019). Predictability of South China Sea Summer Monsoon Onset.
392 *Advances in Atmospheric Sciences*, 36(3), 253-260.
393 <https://doi.org/10.1007/s00376-018-8100-z>
- 394 Merryfield, W. J., et al. (2020). Current and Emerging Developments in Subseasonal
395 to Decadal Prediction. *Bulletin of the American Meteorological Society*, 101(6),
396 E869-E896. <https://doi.org/10.1175/BAMS-D-19-0037.1>
- 397 Moon, J. Y., Wang, B., and Ha, K. J. (2011). ENSO regulation of MJO teleconnection.
398 *Climate Dynamics*, 37(5-6), 1133-1149. [https://doi.org/10.1007/s00382-010-](https://doi.org/10.1007/s00382-010-0902-3)
399 0902-3

- 400 National Academies of Sciences, Engineering and Medicine. (2016). *Next generation*
401 *Earth system prediction: Strategies for subseasonal to seasonal forecasts*.
402 National Academies Press. <https://doi.org/10.17226/21873>
- 403 Orsolini, Y. J., Senan, R., Balsamo, G., Doblas-Reyes, F. J., Vitart, F., Weisheimer, A.,
404 Carrasco, A., and Benestad, R. E. (2013). Impact of snow initialization on sub-
405 seasonal forecasts. *Climate Dynamics*, 41(7-8), 1969-1982.
406 <https://doi.org/10.1007/s00382-013-1782-0>
- 407 Osman, M., and Alvarez, M. S. (2018). Subseasonal prediction of the heat wave of
408 December 2013 in Southern South America by the POAMA and BCC-CPS
409 models. *Climate Dynamics*, 50(1-2), 67-81. [https://doi.org/10.1007/s00382-017-](https://doi.org/10.1007/s00382-017-3582-4)
410 [3582-4](https://doi.org/10.1007/s00382-017-3582-4)
- 411 Qi, X., and Yang, J. (2019). Extended-range prediction of a heat wave event over the
412 Yangtze River Valley: role of intraseasonal signals. *Atmospheric and Oceanic*
413 *Science Letters*, 12(6), 451-457. <https://doi.org/10.1080/16742834.2019.1669408>
- 414 Qin, M. Y., Li, S. L., Xue, Y. F., and Han, Z. (2022). Intraseasonal variability modes
415 of winter surface air temperature over central Asia and their modulation by
416 Greenland Sea ice and central Pacific El Nino-Southern Oscillation. *International*
417 *Journal of Climatology*. <https://doi.org/10.1002/joc.7691>
- 418 Robertson, A. W., Kumar, A., Peña, M., and Vitart, F. (2015). Improving and
419 promoting subseasonal to seasonal prediction. *Bulletin of the American*
420 *Meteorological Society*, 96(3), ES49-ES53. [https://doi.org/10.1175/BAMS-D-14-](https://doi.org/10.1175/BAMS-D-14-00139.1)
421 [00139.1](https://doi.org/10.1175/BAMS-D-14-00139.1)
- 422 Takaya, K., and Nakamura, H. (2001). A formulation of a phase-independent wave-
423 activity flux for stationary and migratory quasigeostrophic eddies on a zonally
424 varying basic flow. *Journal of the Atmospheric Sciences*, 58(6), 608-627.
425 [https://doi.org/10.1175/1520-0469\(2001\)058<0608:AFOAPI>2.0.CO;2](https://doi.org/10.1175/1520-0469(2001)058<0608:AFOAPI>2.0.CO;2)
- 426 Teng, H. Y., and Wang, B. (2003). Interannual variations of the boreal summer
427 intraseasonal oscillation in the Asian-Pacific region. *Journal of Climate*, 16(22),
428 3572-3584. [https://doi.org/10.1175/1520-](https://doi.org/10.1175/1520-3572-3584)

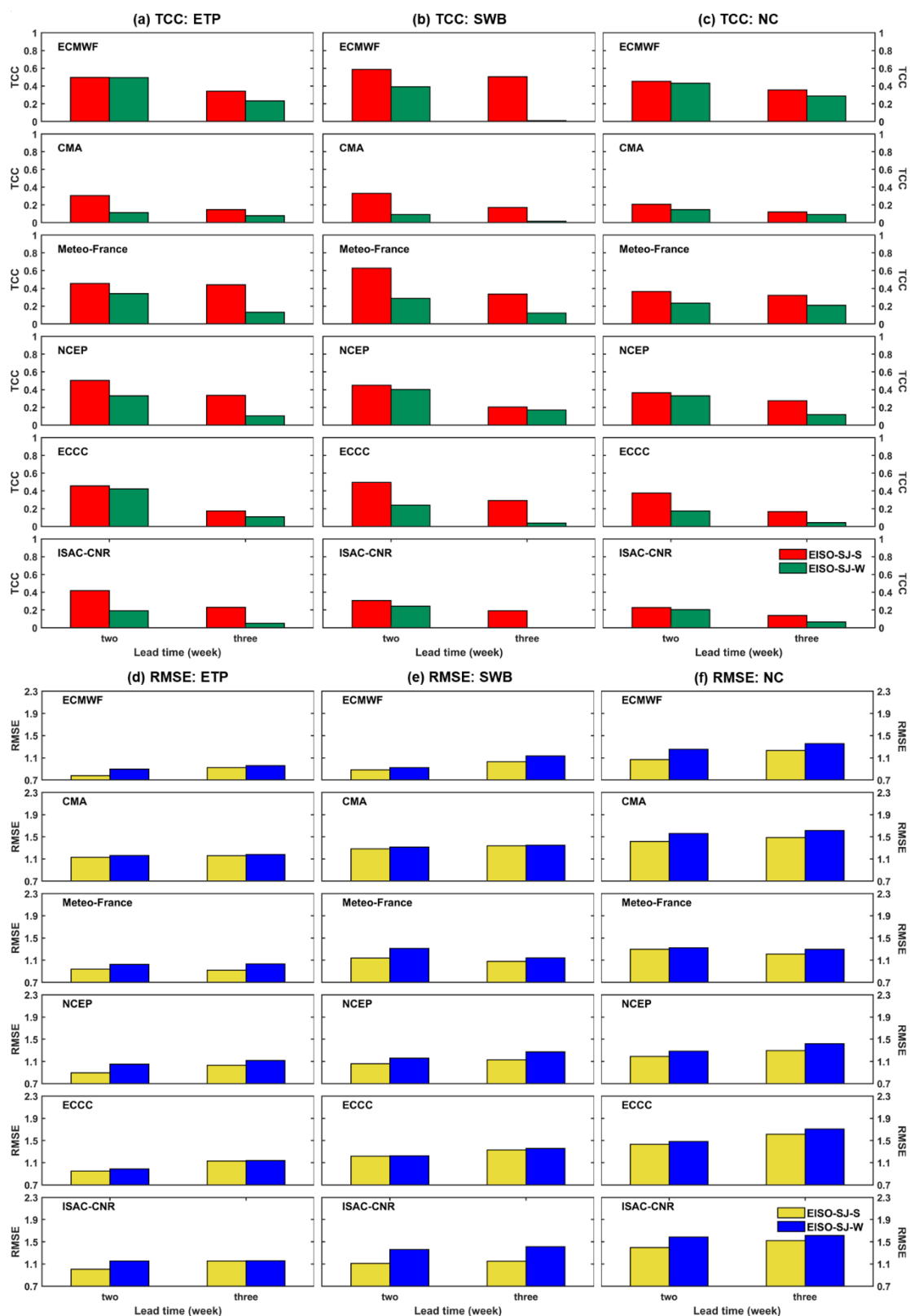
- 429 0442(2003)016<3572:IVOTBS>2.0.CO;2
- 430 Vimont, D. J., Battisti, D. S., and Hirst, A. C. (2001). Footprinting: A seasonal
431 connection between the tropics and mid-latitudes. *Geophysical Research Letters*,
432 28(20), 3923-3926. <https://doi.org/10.1029/2001GL013435>
- 433 Vitart, F., et al. (2017). The subseasonal to seasonal (S2S) prediction project database.
434 *Bulletin of the American Meteorological Society*, 98(1), 163-173.
435 <https://doi.org/10.1175/BAMS-D-16-0017.1>
- 436 Watanabe, T., and Yamazaki, K. (2012). Influence of the Anticyclonic Anomaly in the
437 Subtropical Jet over the Western Tibetan Plateau on the Intraseasonal Variability
438 of the Summer Asian Monsoon in Early Summer. *Journal of Climate*, 25(4), 1291-
439 1303. <https://doi.org/10.1175/JCLI-D-11-00036.1>
- 440 Watanabe, T., and Yamazaki, K. (2014). The upper-level circulation anomaly over
441 Central Asia and its relationship to the Asian monsoon and mid-latitude wave train
442 in early summer. *Climate Dynamics*, 42(9-10), 2477-2489.
443 <https://doi.org/10.1007/s00382-013-1888-4>
- 444 Wu, J., Ren, H., Zhang, S., Liu, Y., and Liu, X. (2017). Evaluation and Predictability
445 Analysis of Seasonal Prediction by BCC Second-Generation Climate System
446 Model. *Chinese Journal of Atmospheric Sciences*, 41(6), 1300-1315.
- 447 Wu, J. T., Li, J., Zhu, Z. W., and Hsu, P. C. (2022). Factors determining the subseasonal
448 prediction skill of summer extreme rainfall over southern China. *Climate*
449 *Dynamics*. <https://doi.org/10.1007/s00382-022-06326-w>
- 450 Xie, J. H., Yu, J. H., Chen, H. S., and Hsu, P. C. (2020). Sources of Subseasonal
451 Prediction Skill for Heatwaves over the Yangtze River Basin Revealed from Three
452 S2S Models. *Advances in Atmospheric Sciences*, 37(12), 1435-1450.
453 <https://doi.org/10.1007/s00376-020-0144-1>
- 454 Xue, Y. K., et al. (2021). Impact of Initialized Land Surface Temperature and
455 Snowpack on Subseasonal to Seasonal Prediction Project, Phase I (LS4P-I):
456 organization and experimental design. *Geoscientific Model Development*, 14(7),
457 4465-4494. <https://doi.org/10.5194/gmd-14-4465-2021>

- 458 Yan, Y. H., Liu, B. Q., and Zhu, C. W. (2021). Subseasonal Predictability of South
459 China Sea Summer Monsoon Onset With the ECMWF S2S Forecasting System.
460 *Geophysical Research Letters*, 48(24). <https://doi.org/10.1029/2021GL095943>
- 461 Yan, Y. H., Liu, B. Q., Zhu, C. W., Lu, R. Y., Jiang, N., and Ma, S. M. (2022).
462 Subseasonal forecast barrier of the North Atlantic oscillation in S2S models during
463 the extreme mei-yu rainfall event in 2020. *Climate Dynamics*, 58(11-12), 2913-
464 2925. <https://doi.org/10.1007/s00382-021-06076-1>
- 465 Yang, J., Bao, Q., Wang, B., Gong, D. Y., He, H. Z., and Gao, M. N. (2014). Distinct
466 quasi-biweekly features of the subtropical East Asian monsoon during early and
467 late summers. *Climate Dynamics*, 42(5-6), 1469-1486.
468 <https://doi.org/10.1007/s00382-013-1728-6>
- 469 Yang, J., Bao, Q., Wang, B., He, H. Z., Gao, M. N., and Gong, D. Y. (2017).
470 Characterizing two types of transient intraseasonal oscillations in the Eastern
471 Tibetan Plateau summer rainfall. *Climate Dynamics*, 48(5-6), 1749-1768.
472 <https://doi.org/10.1007/s00382-016-3170-z>
- 473 Yang, L., and Zhang, Q. (2007). Anomalous Perturbation Kinetic Energy of Rossby
474 Wave along East Asian Westerly Jet and Its Association with Summer Rainfall in
475 China. *Chinese Journal of Atmospheric Sciences*, 31(4), 586-595.
- 476 Zeng, D. W., and Yuan, X. (2018). Multiscale Land-Atmosphere Coupling and Its
477 Application in Assessing Subseasonal Forecasts over East Asia. *Journal of*
478 *Hydrometeorology*, 19(5), 745-760. <https://doi.org/10.1175/JHM-D-17-0215.1>
- 479 Zhang, T. T., Huang, B. H., Yang, S., and Kinter, J. L. (2018). Predictable Patterns of
480 the Atmospheric Low-Level Circulation over the Indo-Pacific Region in Project
481 Minerva: Seasonal Dependence and Intraensemble Variability. *Journal of Climate*,
482 31(20), 8351-8379. <https://doi.org/10.1175/JCLI-D-17-0577.1>
- 483 Zhong, S. S., Wang, H., Chen, B., and Chen, H. (2022). Modulation of the Atmospheric
484 Heat Source Over the Tibetan Plateau on the Intra-seasonal Oscillation of Summer
485 Precipitation in the Yangtze-Huaihe River Basin. *Atmosphere-Ocean*, 60(5), 600-
486 612. <https://doi.org/10.1080/07055900.2022.2077170>



487

488 **FIG. 1.** (a) Variance (shading; unit: $\text{m}^2 \text{s}^{-2}$) and (b) fractional variance (shading; unit: %) of quasi-
 489 biweekly V200 against total V200 variance in boreal summer. Green lines are the summer-mean
 490 U200 contour of 18, 23 and 28 m s^{-1} , which broadly denote the SJ's location. (c) Time series
 491 (unit: m s^{-1}) of domain-averaged quasi-biweekly V200 intensity over the SJ core region. Values
 492 greater (less) than 0.7 times the standard deviation are shaded yellow (green).



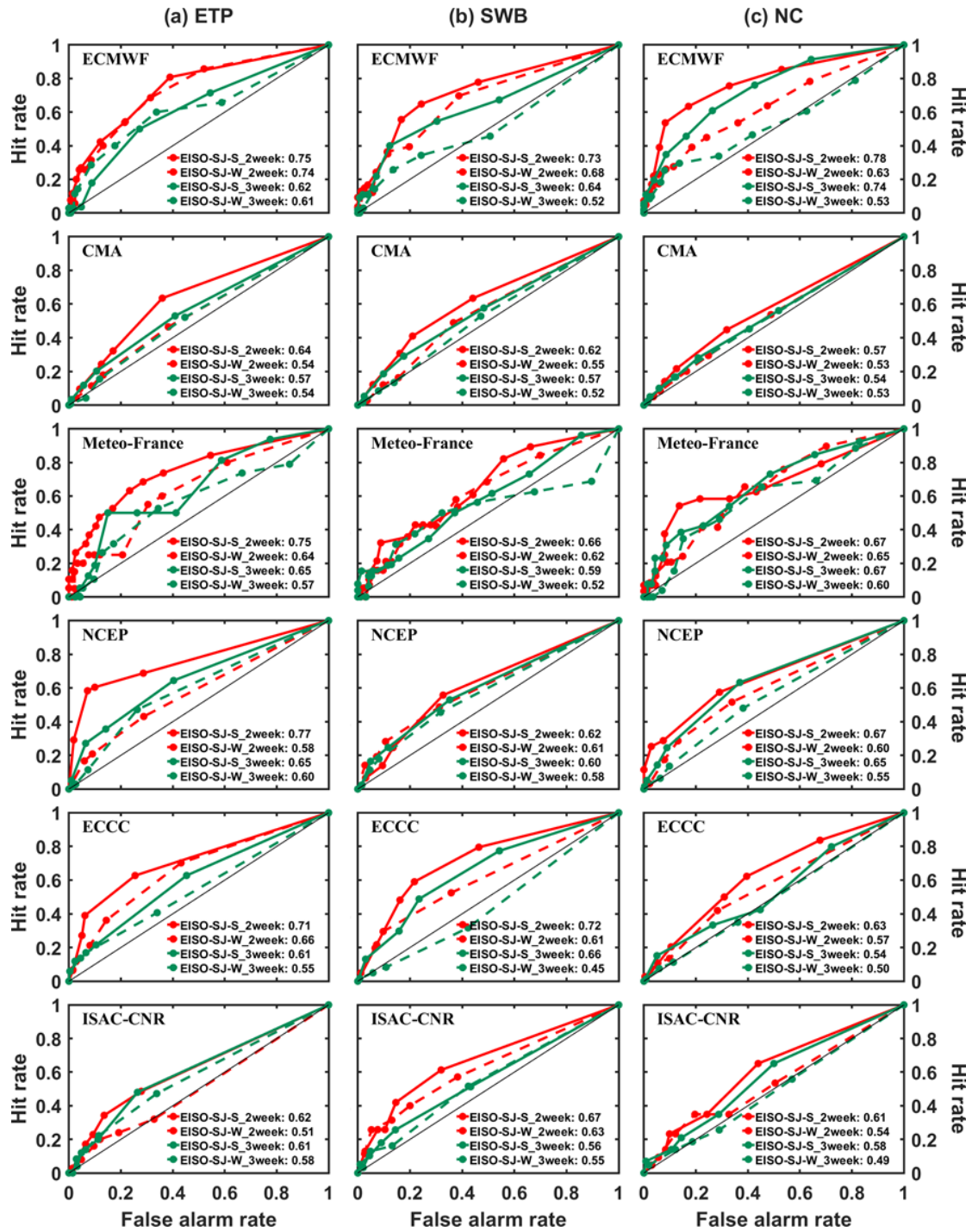
493

494

495

496

FIG. 2. Temporal correlation coefficient (TCC) between the observed weekly SAT anomaly and the predicted ensemble-mean weekly SAT anomaly over the (a) ETP, (b) SWB, and (c) NC with two- and three-week lead times. (d–f) As in (a–c), but for Root Mean Square Error (RMSE).



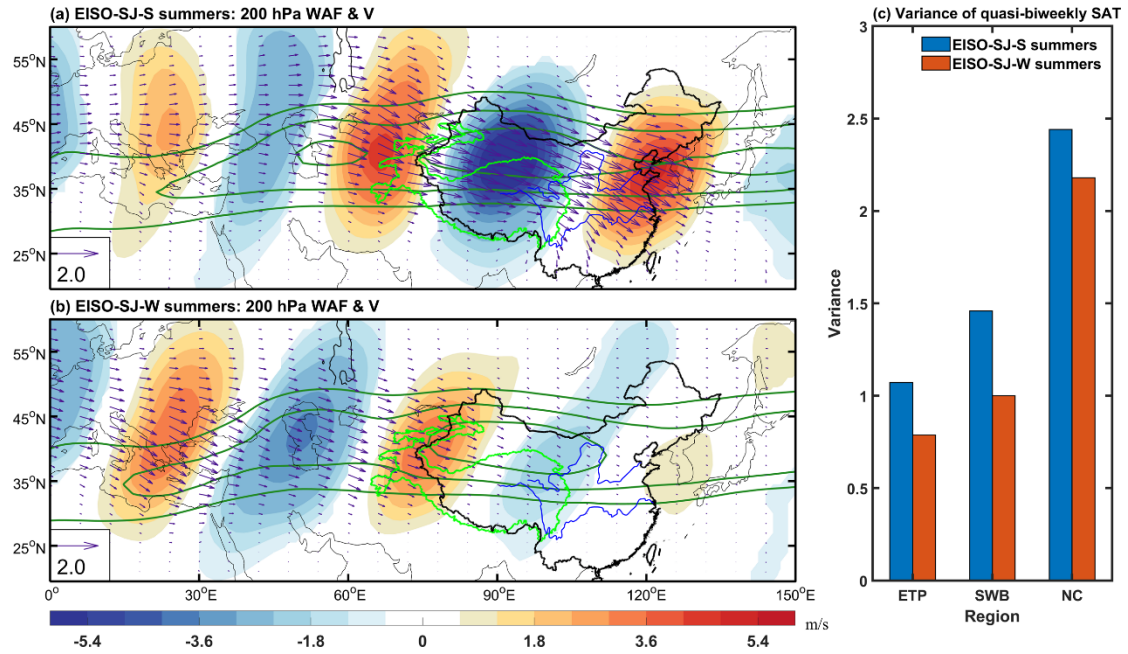
497

498

499

500

FIG. 3. Relative operating characteristics (ROC) curve for predicting above-normal SAT events over the (a) ETP, (b) SWB, and (c) NC from the six S2S models with two- and three-week lead times.



501

502 **FIG. 4.** Regression maps of boreal summer quasi-biweekly V200 (shading; unit: m s^{-1}) and 200
 503 hPa wave activity flux (WAF; vectors; unit: $\text{m}^2 \text{s}^{-2}$) on the first principal component in (a) EISO-
 504 SJ-S and (b) EISO-SJ-W summers. Only values passing the 95% confidence level are plotted. (c)
 505 Variance of quasi-biweekly SAT over the ETP, SWB, and NC in EISO-SJ-S (blue bars; unit: $^{\circ}\text{C}^2$)
 506 and EISO-SJ-W summers (orange bars; unit: $^{\circ}\text{C}^2$).